We are IntechOpen, the world's leading publisher of Open Access books Built by scientists, for scientists

4,800
Open access books available

122,000
International authors and editors

135M
Downloads

Our authors are among the

154
Countries delivered to

TOP 1%
most cited scientists

12.2%
Contributors from top 500 universities

CLARIVATE ANALYTICS BOOK CITATION INDEX INDEXED

WEB OF SCIENCE™

Selection of our books indexed in the Book Citation Index in Web of Science™ Core Collection (BKCI)

Interested in publishing with us?
Contact book.department@intechopen.com

Numbers displayed above are based on latest data collected.
For more information visit www.intechopen.com

15

Applications of Superconductor/Photosemiconductor Contact Structures in Electronics

Viktor V. Bunda and Svitlana O. Bunda
Transcarpathian State University
Ukraine

1. Introduction

The integration of high temperature superconductors(HTSC's) with conventional semiconductor(SeC) - based technology would have important consequences for micro- and cryophotoelectronics, with the promise of high performance hybrid circuits incorporating the best of what superconductors and semiconductors have to offer as well as the possibility for novel devices (Bunda, 1991). The rapid progress in the fabrication of high quality HTSC thin films on oxygen containing substratum such as $SrTiO_3$, MgO, and $LaAlO_3$ has been observed. However, the results on semiconductors like Si, Ge and GaAs has been also reported.

The high temperature superconductors (HTSC's) are considered to be low carrier density materials. Therefore, the light can penetrate the superconductor and can effectively excite the quasiparticles in it. The study of light detection by a "HTSC – photosemiconductor" hybrid contact structures (HCS's) is very perspective for fabrication of multifunctional photonic circuits - high speed detectors with reasonable sensitivity covering a broad electromagnetic spectrum (Bunda et al., 1996). Therefore, for deeper investigation of such type compounds we need fabrication of the HCS's based on oxygen containing photosemiconductor.

Superconductors (SC) have a wide field of applications due to their charge carrier transport properties without energy loss. The charge carriers in the superconducting state are correlated charge carriers (Cooper pairs) as well as uncorrelated ones (quasiparticles). The special magnetic and transport properties of Cooper pairs provide new applications in the field of tunnel contacts, electronic devices and the generation of very high magnetic fields (Akani et al., 1995). Compared to classical ultrasonic sources, superconducting tunnel contacts emit phonons with higher frequency. Therefore, the properties of different HTSC/photosemiconductor heterojunctions are of great interest for the development of new electronic devices such as diodes with very high rectifying parameters (Bunda et al., 2010a) and transistors based on the Josephson field effect (Akani et al., 1995).

In recent years, two-dimensional (2D) nanostructured materials, such as nanoplates and nanosheets, have attracted much attention because of not only their unique electronic,

magnetic, optical, and catalytic properties, which mainly arise from their large surface areas, nearly perfect crystallinity, structural anisotropy, and quantum confinement effects in the thickness (Deng et al., 2008). The potential of 2D nanostructured materials uses for building blocks for advanced materials and devices with designed functions in areas as diverse as lasers, transistors, catalysis, solar cells, light emission diodes, and chemical and biological sensors (Bunda et al., 2010b).

2. Grown and crystal structure of bismuth oxyhalides single crystals

Oxyhalides of bismuth BiOX (X = Cl, Br, I) are very interesting materials which find various applications as X-ray luminescent screens, as anti-Stokes converters, photocatalist, usual luminophors and as photoconductive analyzer of linear polarized radiation in the 0.24 - 1.2μm spectral region. Bismuth oxyhalides provides a very convenient matrix for activation by various rare-earth and 3d-elements: by doping this matrix with different, is possible to obtain a wide variety of optical, luminescent and photoconductive properties. Moreover, these crystals are of essential interest in connection with the research and development work on laser materials. (Bunda et al., 2010b). The great interest for these materials is strongly related to the influence of dimensionality on the behaviour of physical properties (they are 2D structured materials). Bismuth oxyhalides are one of the V-VI-VII group compound semiconductors belonging to the tetragonal system. The structure of BiOX is known to have a layered structure, which is constructed by the combination of the halide ion layer and the bismuth oxygen layer (Bletskan et al., 1973).

The BiOX single crystals are layered 2D structured materials. The crystal structure of BiOX is very similar to the symmetry of space groups P4/*mmm* and/or I4/mmm, where are usual for the $YBa_2Cu_3O_{7-\delta}$ and $Bi(Tl,Hg)_2Sr(Ba)_2Ca_{n-1}Cu_nO_{2n+4}$ HTSC's. Besides, the BiOX crystals, as well as a HTSC's contain oxygen. The thermal expansion and the lattice constants mish-match in the (001) base plane are in good agreement with the same parameters of the HTSC's. Also, the BiOX crystals are good "sparring partners" for the fabrication of "HTSC – photosensitive semiconductor" hybrid contact structure.

Bismuth oxychloride crystals exhibit many intriguing and interesting properties such as photoluminescence, photoconductivity, and thermally stimulated conductivity (Bunda, 1989, 1991, 2005). The luminescent band at 1.6 - 2.2 eV is a result of capture of c-band free electrons by r-centres of recombination. The shape of the absorption edge has been explained by the effect of the laminarity of these crystals. Previous investigations on the crystal structure and morphology of BiOX crystallites showed that they grow usually in the form of platelets with the c-axis normal to the platelets. Investigations on the influence of uniaxial compression on the crystals revealed that they are isotropic along the normal to the layers (Ganesha et al., 1993). Heat conductivity measurements as a function of temperature showed that the electronic component of heat conductivity is negligibly small, since the crystals are nearly insulators in the temperature range 80 -300 K (Bunda, 1991).

The BiOHal samples were prepared in several ways. BiOX pure(starting material for a BiOX single crystals growth) was prepared by dissolving 99,99 pure bismuth oxides in hydrohalides acid, evaporating to form the hydrated halides, dehydrating the latter under vacuum, heating at ~380-700^{o}C in a X_2 atmosphere, cooling to room temperature, and washing the product to remove BiX_3. The BiOX crystals were grown by the vapour gas

transport reaction method in closed volume. The compounds BiOX of 99,99% purity was loaded into a high quality polished quartz ampoule (150-165 mm length and 15 mm diameter; combination of cylinder and cone). The ampoule was evacuated under vacuum of 10^{-4} Torr. After pumping the ampoule was filled with a (H_2O and HX) transport agent (TA). The system of chemical gas-transport reactions are as follows (Bunda, 1991):

$$3BiOX_{(s)} \rightarrow Bi_2O_{3(s)} + BiX_{3(g)}; \quad (1)$$

$$BiX_{3(g)} + H_2O_{(g)} \rightarrow BiOX_{(crystal)} + 2HX_{(g)} \quad (2)$$

$$Bi_2O_{3(s)} + 2HX_{(g)} \rightarrow 2BiOX_{(s)} + H_2O_{(g).} \quad (3)$$

During transport involved three gaseous compounds: H_2O, HX and BiX_3. In the solid state exists a bismuth oxyhalides in polycrystalline and single crystal form. Reaction (1) describes the dissociation process of bismuth oxyhalides. The reaction (2) is a direct gas transport reaction with the water vapour as a transport agent. Reaction (3) describes the halogenation of bismuth oxide to bismuth oxyhalides. The (1-3) reactions cycle is closed and carried to the final transport in a BiOX single crystal of polycrystalline bismuth oxyhalide. The decomposition (1) and hydrolysis (2) reactions of BiOX are endothermic. Therefore, transport is possible only in the $T_2 \rightarrow T_1$ direction ($T_2 > T_1$). A two-zone resistance heated furnace was used for crystal growth. The axis of the ampoule was kept slightly inclined to the horizontal to enhance the transport of the vapour from the source zone to the growth zone during growth. We selected the pressure of transport agent in the ampoule on the basis of optimal mass transfer calculation by the convection method according to the equation (2). The best bismuth oxyhalide crystals were obtained at the 8-10 Torr pressure of transport agent. The some growth parameters of the BiOX crystals obtained are given in table 1.

Substance	Zone temperature (°C)		TA pressure (Torr)	Morphology and size	Growth period (days)
	Source	Growth			
BiOCl	720	600	8-10	Platelets 7x7x3 mm^3	5
BiOBr	700	600	8-10	Platelets 6x7x2 mm^3	6
BiOI	580	450	8-10	Platelets 5x5x1 mm^3	7

Table 1. Temperature of source and growth zones, transport agent pressure and size of BiOX crystals obtained

The crystallinity and morphology of the BiOX crystals was examined by X-ray diffraction (XRD), and field effect-scanning electron microscopy (FE-SEM). The lattice parameters were refined by X-ray powder diffraction data with a Si internal standard (high purity) and by using a least square method. All of the sharp diffraction peaks in the XRD patterns were perfectly indexed as pure phase of BiOCl, in good agreement with the standard JCPDS file (No. 06-0249) of BiOCl. A Laue photograph taken parallel to the large face of the platelets showed clearly a fourfold symmetry axis characterizing (001) planes of a matlockite tetragonal PbFCl--like structure $D_{4h}^7 - P\frac{4}{n}mm$ (No. 129) (Beck & Beyer, 1997) with two formula units in the unit cell and the following atom position (Bercha at al., 1973):

$$2Bi\ in\ position\ (2c)\ (0,1/2,z)(1/2,0,\bar{z})\ of\ 4mm\ (C_{4v})symmetry$$

$$2O\ in\ position\ (2a)\ (0,0,0)\ (1/2,1/2,0)\ of\ \bar{4}2m\ (D_{2d})\ symmetry \quad (4)$$

$$2X\ in\ position\ (2c)\ (0,1/2,z')\ (1/2,0,\bar{z}')\ of\ 4mm\ (C_{4v})symmetry..$$

The position (2a) is always occupied by the smaller anion which is coordinated tetrahedrally by the bismuth cations. The Bi^{3+} ion itself is coordinated ninefold capped quadratic antiprism) and site symmetry has C_{4v}. Fig.1 gives the coordination polyhedron of the cation (d) and a projection of the structure along the [010] direction (b).

An examination of the platelets using a polarizing microscope shows no extinction, thus indicating that the tetragonal *c*-axis is perpendicular to the plane of the platelets. In optical micrograph of a BiOCl crystal multiple growth spiral (two on the same sign) can be seen originating from a growth defect. The growth defect is responsible for the formation of the growth spirals. The observed spirals illustrate once again working of the Burton-Cabrera-Frank (BCF) theory of the crystal growth mechanism (Burton et al., 1951). On the other hand, the layers observed under different magnifications in the SEM of BiOBr and BiOI crystals indicate the layer growth mechanism of these crystals (Ganesha et al., 1993).

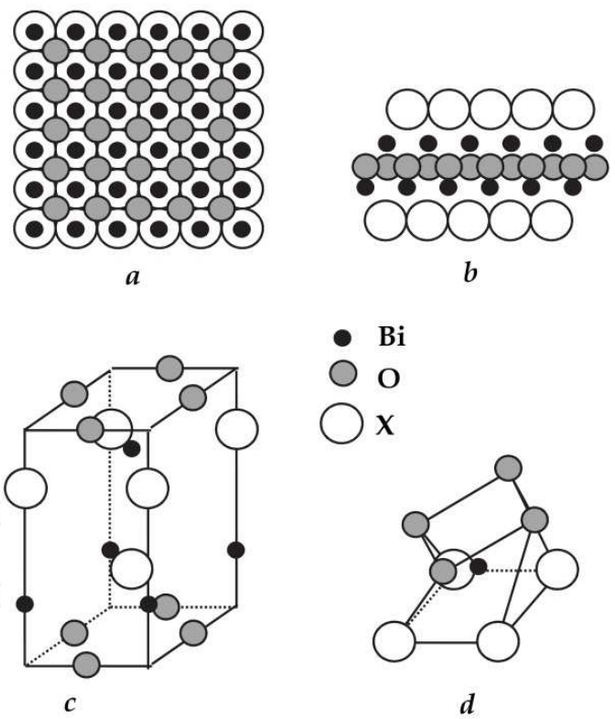

Fig. 1. Crystal structure of bismuth oxyhalides: (a) projection to (001) plane; (b) projection to (100) or (101) plane; (c) clinographic projection of the unit cell; (d) coordination polyhedron of the bismuth

Fig.1a shows the clinographic projection of the unit cell of BiOX crystals. Each Bi atoms is eight-coordinated by four O atoms and four X (halogen) atoms in the form of an asymmetric decahedron (Keramidas et al., 1993). Each atom (Bi, O, X) occupies a special position with

multiplicity 2. The faces of the decahedron are 2 rectangles (O-O-O-O, X-X-X-X, which are parallel to the (110) plane and 8 isosceles triangles (four X-O-X and four O-X-O). The decahedra are linked to each other by a common O-X edge along the a and b axes forming infinite layers. The coordination of O and X are follows. Each O atom is linked to four Bi atoms and forming a tetragonal pyramid with the O atom at its apex. Also each X atoms forms with the neighbouring Bi atoms tetragonal pyramid with the X atom at its apex. Neighbouring decahedra form layers along (001) which are connected by common O-X edges. Neighbouring layers of decahedra are connected by common O-O or X-X edges.

The X atom is bonded with four Bi atoms in a planar square to form a pyramid and with its nonbonding (lone pair) electrons pointing to the other side of the square. These nonbonding electrons convert the three-dimensional fluorite-like structure into a two-dimensional layered structure. In the three-dimensional Bi_2O_3, the Bi atoms are coordinated to six O atoms. This structural difference between them is the major reason for BiOX to have a wider optical band-gap. As shown in the fig. 1, the [BiOX] layers are stacked together by the nonbonding (van der Waals) interaction through the X atoms along the c-axis. Therefore, the structure is not closely packed in this direction. When one photon excites zone electron from X np states (n = 3, 4, 5 for Cl, Br, I respectively) to Bi 6p states in BiOX, one pair of a hole and an excited electron appear. The layered structure BiOX can provide the space large enough to polarize the related atoms and orbitals (Zhang et al., 2006). The induced dipole can separate the hole–electron pair efficiently, enhancing photocatalytic activities. BiOX has an indirect-transition band-gap so that the excited electron has to travel certain k-space distance to be emitted to valence band (Table 2). Therefore, the BiOX single crystals can be described as 2D structured materials.

Substance	Lattice constants, Å		Relaxed atomic position		Θ_D, K	E_g, eV
	a	c	z	z'		
BiOCl	3.883	7.347	0.645	0.170	205	3.455
BiOBr	3.915	8.076	0.653	0.154	168	2.924
BiOI	3.984	9.128	0.668	0.132	146	1.89

Table 2. Lattice parameter (a, c) , relaxed atomic position (z, z'), Debye temperature (Θ_D) and band gap (E_g) of bismuth oxyhalide crystals (Bunda et al., 2011)

3. Fabrication and classification of HTSC/photosemiconductor hybrid contact structures

In this capture we report the formation process of "ceramics HTSC($YBa_2Cu_3O_{7-\delta}$)/thin film SeC (BiOX)" hybrid contact structures(HCS). The choice of the structure "HTSC-ceramic - SC-thin film" was due to the nonstability of the HTSC- film parameters. The layers of bismuth oxyhalogenides were prepared in the three ways (Bunda, 1991): a) the thermal discrete evaporation in the oxygen atmosphere (p=7-10 Torr); b) the laser impulse evaporation (the laser type of LTYPTSH-500; λ=0.53 μm; ω=50 Hz); c) the deposition by the method of gas chemical transport reactions in the quasiclosed volume. The films were characterized by qualitative X-ray analysis (powder diffraction measurements, using CuK_α-radiation), and by scanning electron microscopy with energy disperse chemical analysis SEM-EDS (for phase composition information). Preliminary $YBa_2Cu_3O_{7-\delta}$ ceramic were overreached in oxygen ions plasma atmosphere for reconstruction of the superconducting

properties of disturbed surface layer. The hybrid contact structures were finally annealed at a temperature T=230-250^{o}C (recrystallization and thermal relaxation procedure). Surface factor of prepared samples was controlled by scanning electron microscopy (SEM).

In the "HTSC - SeC" system can be formed three principal types of HCS's (Bunda et al., 1996): tunneling(1), proximity(2) and combined(3). In the case $d \gg \xi_p$ (ξ_p- the value of coherence length in the HTSC; d- the thickness of insulator(I) layer between super- and semiconductor) the electrical properties of "HTSC - SC" junction are mainly determinate by the parameters of the transition layer d. At d ~ ξ_p take place both the HTSC-I-SC junction (HCS of type 1) with high (ρ_d > 10^3 - 10^5 Ω·cm) values of the differential resistance ρ_d (at the bias voltage $V_{tr} \rightarrow 0$) and proximity contact(HCS of type 2) with the $\rho_{d \rightarrow} 0$. In the case d ~ ξ_p and 0< ρ_d< 10^3 - 10^5 Ω·cm take place HCS of type 3 - combined "proximity- tunnelling" junction (Bunda et al., 1996). The classification of principal possible types of "HTSC-SC" hybrid contact structures is show in the table 3.

Type of structure	Modification		Method of fabrication	ρ_d (Ω·cm)
	HTSC	SeC		
1. Van der Waals press contakt (type 1)	Ceramics	Crystals	Press optical contact with the polished ceramics	$10^3 \div 10^{12}$
2. Heterojunction (type 1, 3)	Ceramics	Thin films	Thermal discrete evaporation; laser ablation	$10^2 \div 10^5$
3. Heterojunction (type 1, 3)	Ceramics	Crystals	Chemical gas transport reactions	$10^1 \div 10^5$
4. Heterojunction (type 2,3)	Films	Films	Laser ablation; magnetron sputtering	$10^{-1} \div 10^2$
5. Heterojunction (type 2)	Films	Crystals	Laser ablation; magnetron sputtering	$10^{-3} \div 10^1$
6. Homogeneous p-p$^+$-junction in HTSC ceramics (type 1-3)	HTSC ceramics with oxygen concentra-tion gradient		Oxygen ions implantation	$10^{-2} \div 10^3$
7. Homogeneous p-p$^+$-junction in HTSC single crystals (type 1-3)	HTSC single crystals with oxygen concen-tration gradient		Oxygen ions implantation	$10^{-3} \div 10^2$

Table 3. Classification and methods of fabrications HTSC/SeC hybrid contact structures

The realization of "HTSC-SC" HCS's assumes the following conditions (Bunda et al., 1996):

- semiconducting layers should be hole conductivity type (p-type; only for the HCS's of type 1). For the semiconductors with the compensation type of conductivity the degeneracy($\zeta_p = E_F - E_v < 0$) is necessary;
- the thermal expansion and the lattice constants mish-match in the (001) base plane should not exceed the values of 15% and 2-5%, respectively;
- the presence of oxygen ions in the anion sublattice of semiconductor is desirable;
- the crystal structure of semiconductor should be very similar to the symmetry of space groups P4/*mmm* and/or I4/mmm, where are usual for the $YBa_2Cu_3O_{7-\delta}$ and $Bi(Tl,Hg)_2Sr(Ba)_2Ca_{n-1}Cu_nO_{2n+4}$ HTSCs.

Some progress has been made in the growth HTSC thin films on Si and on GaAs (Shiwagan et al., 2002). All successful growths have used intermediate buffer layer between the HTSC films and semiconductor substrates. The major problem in using the semiconductor substrates is the substrate-film inter-diffusion during the in-situ depositions rn addition to the formation of micro cracks in the films due to a relatively large difference rn thermal expansion coefficients between the semiconductor and HTSC. After the deposition of CdSe the critical transition temperature of HgBaCaCuO films was found be increased from 115 K with J_c = 1.7 x 103 A/cm² to 117.2 K with J_c = 1.91 x 103 A/cm². When the heterostructure was irradiated with red He-Ne laser (2 mW), the T_c was further enhanced to 120.3 K with J_c = 3.7 x 103 A/cm² (Shiwagan et al., 2002, 2004). The resistivity is decreased after the laser irradiation, but the nature of variations in resistivity with temperature remains similar to that of without laser irradiated samples. The decrease rn resistivity is attributed to increase in charge carriers in the heterostructure during laser irradiation. The CdSe has the direct band gap 1.74 eV and hence the laser source with energy 1.95 eV greater than band gap of CdSe was selected. Hence during the irradiations, the electron-hole pair generates in the CdSe sample individually at the junction of the heterostructure. As authors (Shiwagan et al., 2004) of work specify, the built-in-junction potential (n) CdSe and (p) HgBaCaCuO heterojunction the electron-hole pairs generated at interface could not recombine, rather holes are transferred to the superconductor region where they can be further trapped into CuO_2 layer and hence there is increase in conductivity.

4. Mechanism of photoconductivity in BiOX (X=Cl, Br, I) single crystals

The spectral dependences of the steady-state photocurrent (photoconductivity) were recorded using a LOMO MDR3 monochromator. Low temperatures were obtained by mounting the sample in an UTREKS continuous flow cryostat. The decay time measurements were performed using pulse UV- laser LGI-21 (pulse width 8-9 ns; excitation wavelength λ=0.337 nm; filters UFS-2 and UFS-6 were used). The change in the intensity was done by a platinum reducer (Bunda, 1989, 2005).

The original specimens had a dark resistivity of ρ_d = 10^{10} to 10^{11} Ω·cm and significant photosensitivity (Bletskan ey al., 1973). At a temperature 293 K and an illumination of 10^4 1x, the ratio ρ_d/ρ_{ph} (ρ_{ph} is the resistivity in the light) reached 10^3; cooling of the specimen led to an increase of 3-4 orders of magnitude in the steady-state photocurrent such that at 90 K, ρ_d/ρ_{ph} > 10^7. Thus, there was an intense temperature (T) suppression of the photocurrent (see fig. 2a).

The spectral dependence of the photoconductivity $\sigma_{ph}(h\nu)$ for a typical specimen of BiOCl recorded at 95 K (curve 1) and 293 K (curve 2) is illustrated in Fig. 2b. In addition to the intrinsic maximum $h\nu_1$= 3.54 eV (350 nm) which corresponds to the band gap of E_g = 3.5 eV at T = 100 K a significant impurity photoconductivity is observed due to the transfer of an electron from the *r* centre to the conduction band (Bunda, 1989). On heating, the main maximum is shifted towards the long-wave side at a rate of dE_g/dT= -6.3·10^{-4} eV/K, while the photoconductivity in both the impurity and intrinsic regions falls sharply. The depth of the level which produces the impurity photocurrent maximum was found to be E_{cr}^0=2.2 eV Bunda, 2005)..

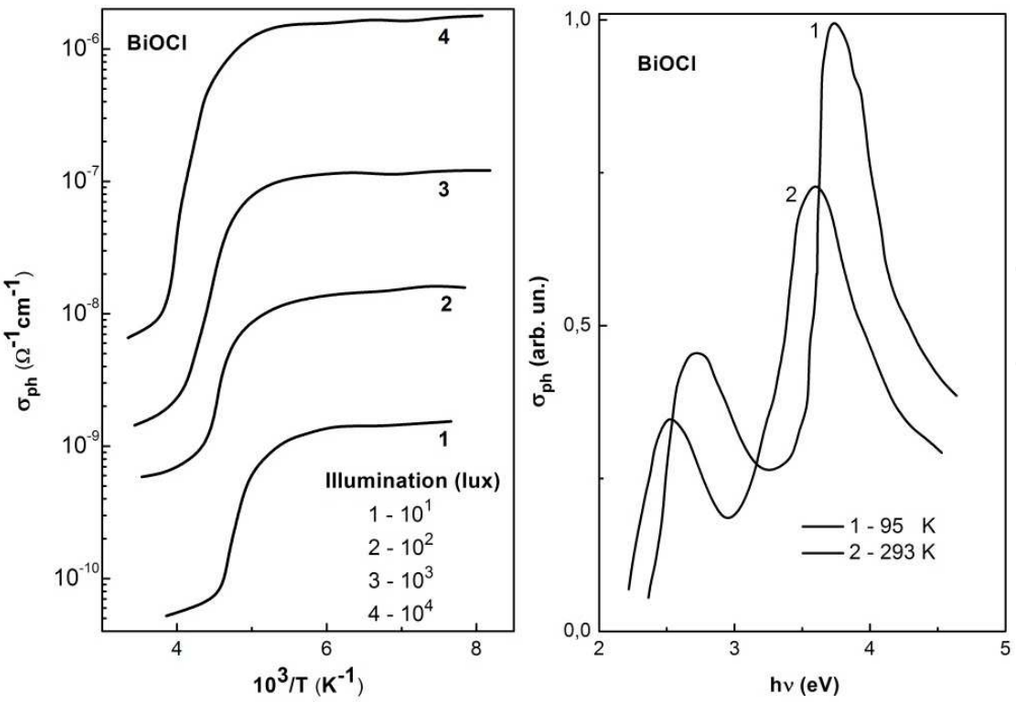

(a) (b)

Fig. 2. The temperature dependence (a) and the spectral dependence (b) of photoconductivity BiOCl single crystal

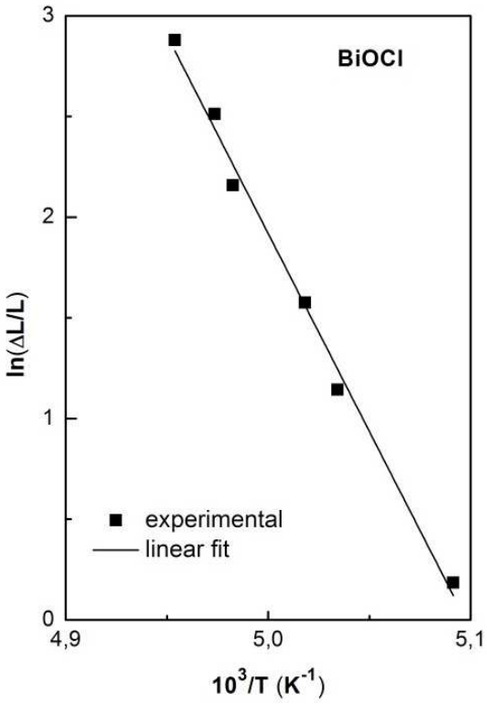

Fig. 3. Temperature dependence of the $\ln(\Delta L/L)$ value

The lux-ampere characteristics of the photocurrent (fig.3) at low temperatures up to the region of T-suppression are linear in the experimental illumination range α=1 [$\alpha = \frac{dL}{dI_{ph}}\frac{L}{I_{ph}}$); $I_{ph} \sim L^{\alpha}$]. In the T-suppression region the lux-ampere characteristics become superlinear and the value of α depends on the concentration of photocurrent carriers *n*, at a fixed temperature. The maximum value of α observed in the experiment reached α = up 3 to 4. At low temperatures, an optical IR suppression of the photocurrent was observed (Bletskan et al., 1973).

A study of the photoconductivity kinetics was made in the linear regime: $\Delta n \ll n$, where Δn is the change in n caused by a short pulse of light in the intrinsic excitation region. The curve of the decay of the photocurrent during the illumination by a pulse of intrinsic light consisted, of course, of two sections with clear by different times : $\tau_r = (2.5 - 6.6) \cdot 10^{-3}$ and $\tau_s = (0.8 - 4) \cdot 10^{-5}$ s.

The presence of temperature and IR suppression of the photocurrent, the superlinearity of the lux-ampere characteristics, and the two sections observed on the relaxation curves of the photoconductivity, indicate unequivocally that in these particular crystals, the recombination processes are determined by two types of centres: "sensitizing" *r* centres and fast *s* centres.

The energy distance of the *r* centres from the valence band is E_{Vr}^{T} and the thermal value was determined from the dependence on the carrier concentration of the temperature at which the thermal suppression of photocurrent begins as in (Bletskan et al., 1973): E_{Vr}^{T}=1.3 eV.

Another more accurate method of determining E is to measure the dependence of $\Delta L/L$ on 1/T, where ΔL is the change in intensity of the exciting light L which is necessary for maintaining the electron concentration *n*, with a change in the temperature in the T-suppression region,

$$\frac{\Delta L}{L} = \frac{g_s B}{C_{rn} n} = g_s Q_v \frac{C_{rp}}{n C_{rn}} \exp(-\frac{E_{vr}^{T}}{kT}), \tag{5}$$

where g_s is the portion of the total carrier-recombination current passing through the *s* centres; g_r is the portion passing through the *r* centres; C_{rp} and C_{rn} are the probabilities of hole or electron trapping at an r centre; and Q_v is the static factor of the valence band. From the curve of $\ln(\Delta L/L)$ (Fig. 3) was determined E_{Vr}^{T} = 1.3 eV (Bunda, 1989, 2005).

Next, we present results of the study of photoconducting spectra anisotropy of the BiOX single crystals, obtained with the polarization of electrical vector $\vec{E}$ of the electromagnetic wave parallel and perpendicular to each of the two axes ([100] or [010]) of the unit cell. The BiOHal compounds are broad-band (1.80 - 3.50 eV) photo-semiconductors. The maxima of their photoconductivity are in the interval of 0.24-1.2 μm and theirs photosensitivity's are $S = \sigma_{ph}/\sigma_d = 10^4 - 10^8$ arbitrary units at the temperature 80K (Fig. 4). The anisotropy of photoconducting spectra is believed to be the results of the layer matlockite-type (PbFCl) crystal structure of all bismuth oxyhalide compounds.

The coefficient of photopleochroism was calculated as

$$P = \frac{I_{\parallel} - I_{\perp}}{I_{\parallel} + I_{\perp}} \cdot 100\% , \tag{6}$$

where $I_{//}$ and $I_{\perp}$ is the photocurrent values at the $\vec{E}//[100]$ and $\vec{E}\perp[100]$ light polarization, respectively.

The position of electrical vector $\vec{E}$ can be varied either by rotating of the crystal. Anisotropy in 3 - 5 times was observed for the photosensitive value S. The change in light polarization at the 90 degrees (from [100] to [010] crystallographic direct) leads to the change in the photoconductivity of 50-100 units (Fig. 5).

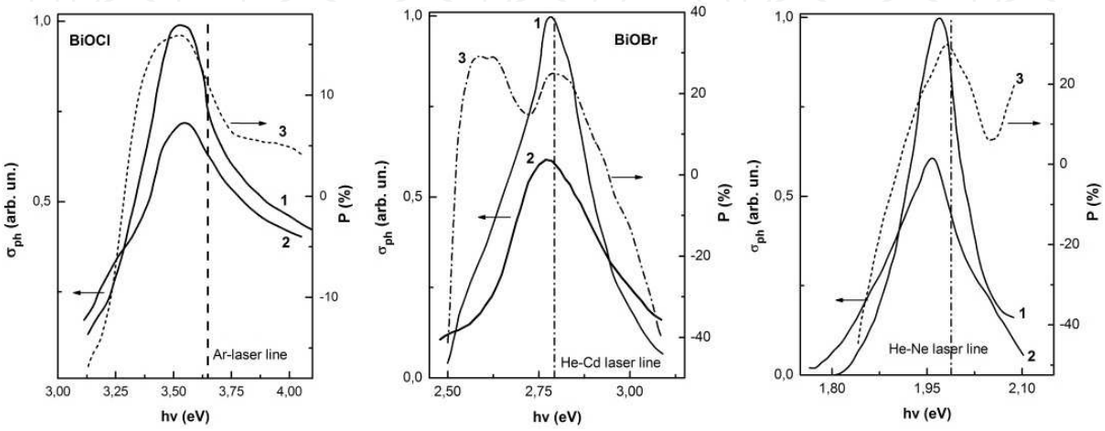

Fig. 4. Photoconductivity and photopleochroism spectra of (a) BiOCl, (b) BiOBr and (c) BiOI single crystals at different light polarization and temperature 80K

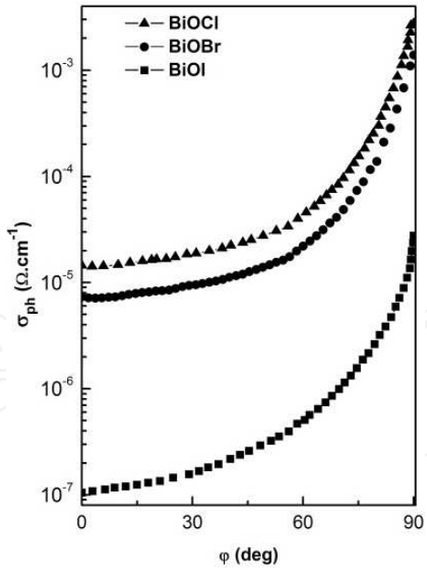

Fig. 5. Angular dependencies of photoconductivity of BiOX single crystals

The temperature region of BiOX based photoresistors is in the range 80-400K. They are stable in air, and their parameters do not depend on the environment, which eliminates the need for sealing. It was established experimentally that the adsorption of oxygen leads to a slight increase even values of photosensitivity (Bunda, 1989, 2005). Other adsorbents do not

cause changes in the photoelectric properties. Crystal structure of the sample reduces the intrinsic noise of the radiation detector. The functional photoresistors based on BiOX single crystals, included in electronic circuits as a two-terminal networks, what is their great advantage. They can follow the rotation of polarization plane or work in schemes of the maximum signal finding. Besides, the BiOX crystals can be used as photo-potentiometers. The selectivity of BiOX spectral characteristics make them good radiation detectors of the nitrogen, argon and helium-cadmium lasers, as well as some of the semiconducting light-emitting diodes (LEDs). Therefore, they can be used in optoelectronic circuits in conjunction with these lasers and LEDs.

5. Energy structure and tunnelling effects of HTSC/BiOX hybrid contact structures

The bismuth oxyhalide single crystals are very good "sparring partners" to create a HTSC/BiOX hybrid contact structures. This is for the following reasons:

1. The good thermal expansion and lattice constants mishmash (15% and 3% respectively) for the base planes (001) is observed.
2. The BiOX compounds have a layered structure and can be easily crystallized as an ultra-thin (0.25-0.5 μm) single crystalline layers on the HTSC substratum's using the method of chemical gas transport reactions.
3. The BiOX crystals are broad-band (E_g=1.85-3.65 eV) photosemiconductors. The maximum of their photoconductivity are in the 0. 24 - 1. 0 mkm interval and theirs photosensitivity's are $S = \sigma_{ph}/\sigma_d = 10^4 - 10^8$ at the temperature 80K.
4. The bismuth oxyhalide single crystals can be easily intercalated (5-7 weigh %) and doped (0. 01-3%) by the 3d- and 4f- elements. That leads to the stable p-type conductivity, and the level of degeneration $\zeta = E_v - E_F$ (E_v – valence band; E_F – Fermi level position) can be controlled.
5. The BiOX layered compounds contain not less than two elements - the cation (Bi^{3+}) and anion (O^{2-}), like in superconductors $YBa_2Cu_3O_{7-\delta}$ or $Bi_{2-x}Pb_xSr_2Ca_{n-1}Cu_nO_{2n+4}$. Therefore the contamination process of the heterojunctions during the formation procedure are absent.

The unique temperature behaviour of the HCS's resistance consists in an N-shape anomaly around the superconducting transition temperature (interval 85-105K; T_c=92K; fig.6). The temperature dependence of the BiOCl:Ti semiconductor resistance can be described by the exponential function $\rho(T) = \rho_0 \exp(-E_g/kT)$, where E_g=2.8 eV and ρ_0=10^2-10^7 Ω·cm, depending on the activation regimes.

The detailed consideration of the temperature dependence of the heterojunction resistance in both directions (curves 1 and 2 on fig.6) shows the anomaly of heterojunction resistance in the narrow temperature interval above T_c (ΔT=5K). The resistance first decreases down to ρ_{min} at T=T_c+2K and then rapidly increases to the maximum at T=T_c+5K. Subsequently, the resistance of heterojunction decreases according to the exponential dependence up to the room temperature. So the temperature dependence of $YBa_2Cu_3O_{7-\delta}$/BiOCl:Ti heterojunction resistance were characterized strongly pronounced N-shaped character in the narrow temperature interval above the superconducting transition. Fig. 6 shows the considerable

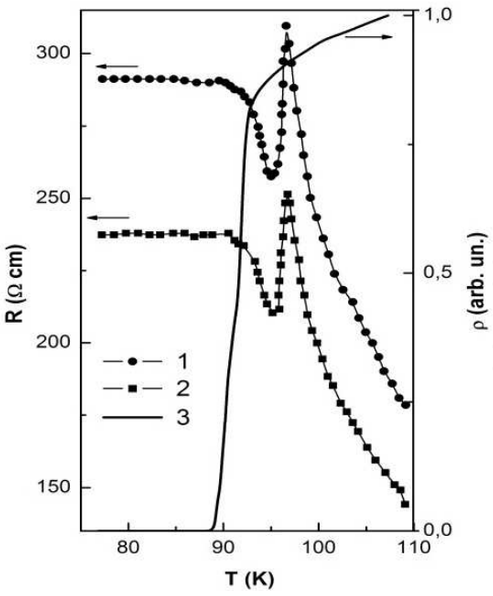

Fig. 6. Dependencies of the resistance R versus temperature for the $YBa_2Cu_3O_{7-\delta}$/BiOCl:Ti HCS along the semiconductor layer in (100) plane (curve 1) and trough the junction (perpendicular to (001) plane; curve 2). The curve 3 characterize the temperature dependence of $YBa_2Cu_3O_{7-\delta}$ ceramics resistance

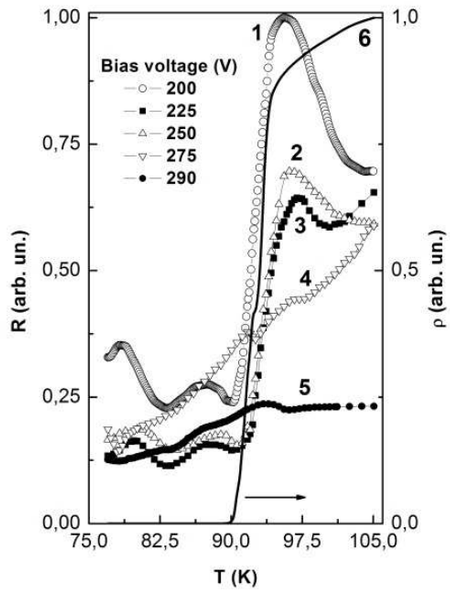

Fig. 7. Temperature dependencies of $YBa_2Cu_3O_{7-\delta}$/BiOI hybrid contact structure resistivity at the different values of bias voltage along the (100) plane. The curve 6 characterize the temperature dependence of $YBa_2Cu_3O_{7-\delta}$ ceramics resistance difference in the values of maximally resistance's (amplitudes of the peaks) and N-anomalous temperature width for the curves 2 and 3 (see fig.6). It is interesting that these anomalies in the $\rho(T)$ dependence appear at the T>T_c, and the appreciable deviation (decreasing) of the differential resistance appeared long before the approach to T_c (at T=85K).

Fig. 7 show the dependencies of resistance versus temperature for the hybrid contact structure $YBa_2Cu_3O_{7-\delta}$ (ceramics)/BiOI (single crystals) along the (001) plane of semiconductor at the different values of the bias voltage V_{tr}. We observed very similar to $YBa_2Cu_3O_{7-\delta}$/BiOCl:Ti heterojunction "resistivity - temperature" behaviour (see Fig.6). Note the characteristic features of these curves. The first, in T_c vicinity the N-like anomaly of electrical resistance is observed (these anomaly is not dependent on the geometry of the measurements). Second, the amplitude jumps of the resistance *R(T)* (and width of derivate negative value *dR(T)/dT*) was strongly dependent on the applied bias voltage. Third, exist the areas of bias voltage where the resistance jumps have maximum amplitude. For planar and through geometry them are 90-100 V and 220-255 V, respectively. Fourth, in the T_c vicinity the anomalies of thermopower are observed.

The red He-Ne laser (with λ = 632.8 nm, E = 1.95 eV and power P = 1.5 mW) was irradiated onto BiOI surface of $YBa_2Cu_3O_{7-\delta}$/BiOI heterostructure, for the 1 hour. The variation in the G_T/G_{300K} normalized conductance during laser irradiation was measured as a function of temperature and is shown in figure 8. It can be excitingly observed that the T_c is further increased from 92K to 94.5 K and critical current value J_c measured at 80 K is $1.85x10^3$ A/cm². Here, the increase superconducting parameters can only be attributed to the increase in carrier concentration when the sample was irradiated by laser having the energy greater than the band gap of semiconductor (Shiwagan el al., 2002).

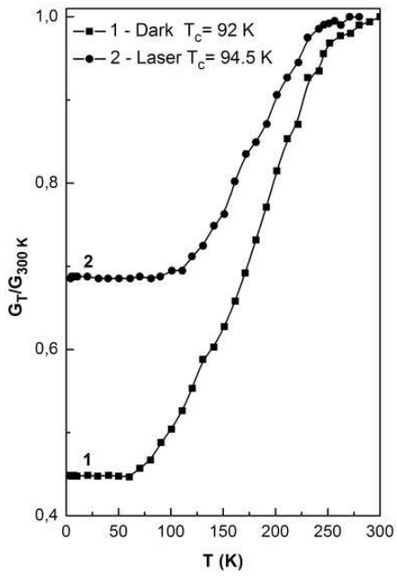

Fig. 8. Variation in normalized conductance of $YBa_2Cu_3O_{7-\delta}$/BiOI heterostructure in (1) dark; and (2) under laser irradiation

The increase in superconducting parameters after laser irradiation is attributed to the microlevel dislocations due to lattice mismatch, attachment to the nonstoichiometric oxygen present on the BiOI surface, development of a diffusion region in semiconductor side of the interface (Shiwagan et al., 2004).

The proposed energy band diagrame for the $YBa_2Cu_3O_{7-\delta}$/BiOCl:Ti hybrid contact structures is shown on the Fig. 9. It is assumed that the semiconductor is characterized by a p-type conductivity (Alfeev et al., 1990,1991). He is in a degeneration state. The degree of degeneration $\zeta_p = E_v - E_F$ is much more than the $2\Delta_0$ twice energy gap value ($\zeta_p \gg 2\Delta_0$).

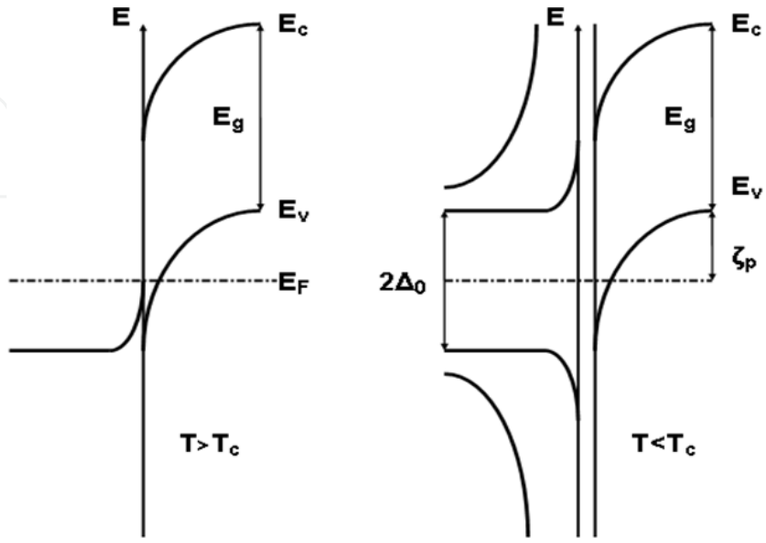

Fig. 9. The energy band diagram of "HTSC/SeC" heterojunctions

At temperatures $T < T_c$ we observed the changes of elementary excitations spectra of HTSC - formation of the $2\Delta_0$ energetic gap near the Fermi level. The unique of the temperature dependence $YBa_2Cu_3O_{7-\delta}$ /BiOCl:Ti junction resistance and negative differential resistance values in the current–voltage characteristics around the superconducting transition can be related to quantum tunnelling of quasiparticles through the junction. The E_F Fermi surface divides basic and excited states of quasiparticles (Cooper's pairs). This provides the possibility for the mutual control of their properties.

Single particle tunnelling can be described by the tunnelling Hamiltonian (Tinkham, 1996)

$$H_T = \sum_{\sigma kq} T_{kq} c_{kq}^* c_{kq} + h.c. \tag{7}$$

In eq. (7) the specific details of the tunnelling barrier are included in the phenomenological tunnelling matrix element T_{kq} with wave vectors k and q of the electrons of one of the electrodes. The tunnelling process itself is described by the annihilator c_{kq} which removes an electron with wave vector k and spin σ, and the creator c_{kq}^* generating an electron with q on the other electrode (Kleine, 2010).

Besides the tunnelling probability given by $|T_{kq}|^2$, the tunneling current is governed by the number of quasiparticles trying to tunnel and on the available states into which they can tunnel. This is accounted for by the density of states of both electrodes $N_{1,2}$ and their occupation given by the Fermi function *f(E)*. Multiplying this with the tunnelling probability leads to the following expression for the tunnelling current

$$I(U) = A|T_{kq}|^2 \int_{-\infty}^{+\infty} N_1(E) N_2(E + eU)[f(E) - f(E + eU)]dE \tag{8}$$

with A as a constant of proportionality (Tinkham, 1996).

In the case of a normal metal/semiconductor (NSeC) tunnel junction applying a voltage shifts the Fermi energy of the electrodes by eU with respect to each other, which results in a net tunnelling current and a normal state conductance $G_{nn} \neq 0$. This current increases with bias since on the one hand more quasiparticles can participate in tunnelling and on the other hand more empty states are available. Therefore, as long as the barrier is not affected by the bias, eq. (8) gives a linear current vs. bias (I-U) characteristic in NSeC systems with $I(U) = U/R_T$. R_T is called tunnelling resistance and is proportional to $1/|T_{kq}|^2$.

Within the BCS theory a temperature dependent energy gap $\Delta(T)$ can be deduced from the excitation spectrum of a superconductor exhibiting its largest value at T = 0. With rising temperature, the energy gap shrinks and vanishes at $T = T_c$. The energy gap $2\Delta(T)$ corresponds to the energy which is necessary to split up a Cooper pair and create two single quasiparticles in the superconductor. These quasiparticles exist above the gap as exited states. The size of the energy gap at T=0 is related to T_c via $\Delta(0) = 1.764kT_c$. Close to T_c the temperature dependence of the energy gap is (Tinkham, 1996)

$$\Delta(T) \approx 1.74\Delta(0)\sqrt{1-\frac{T}{T_c}}. \tag{9}$$

The transition from normal to superconducting state leads to a change of the density of states N as a direct consequence of the emergence of the energy gap. The superconducting density of states N_s for quasiparticles at energy E reads (Buckel & Kleiner, 2004)

$$N_s(E) = \begin{cases} N_n(E_F) \cdot \frac{|E-E_F|}{\sqrt{(E-E_F)^2-\Delta^2}} & for\ |E-E_F| \geq \Delta \\ 0 & for\ \ |E-E_F| \leq \Delta \end{cases} \tag{10}$$

where N_n is the normal metal density of states at $T > T_c$ and E_F the Fermi energy. It follows from eq. (10) that no single particle states exist in the energy interval $E_F \pm \Delta$, whereas N_s exhibits a singularity at the gap edges and reduces to N_n at larger energies, see Fig. 9.

In superconducting tunnelling spectroscopy one mostly deals with semiconductor/superconductor (SeCSC) tunnel junctions which exhibit nonlinear $I-U$-characteristics. For an applied bias $|U| < \Delta/e$ and $T = 0$ no single particle tunnelling is possible, because no available excitation states do exist in the superconductor ($N_s = 0$), see eq. (10). The characteristic strong increase of the tunnelling current at $|U| = \Delta/e$ is due to the singularity in N_s and the resulting large number of unoccupied states, see Fig. 9. For $|U| \gg \Delta/e$ the $I-U$ - characteristic resembles the one of an SeCN junction since N_s is similar to N_n in this energy range. With eq. (8) the bias dependence of the tunnelling current of an SeCSC junction is described by (Kuznetsov, 2002, 2004)

$$I(U) = A|T_{kq}|^2 N_1(0) \int_{-\infty}^{+\infty} N_{2s}(E)[f(E) - f(E+eU)]dE. \tag{11}$$

When taking the derivative of eq. (11) with respect to the applied voltage, one gains the following expression for the differential conductance (Tinkham, 1996)

$$G_{ns} = \frac{dI_{ns}}{dU} = G_{nn} \int_{-\infty}^{+\infty} \frac{N_{2s}(E)}{N_2(0)} \left[-\frac{\partial f(E+eU)}{\partial(eU)}\right] dE \tag{12}$$

which directly gives N_s for $T = 0$. Temperature dependent STS measurements, as shown in Figures 6 and 7, exhibit smeared features with increasing T, because the energy gap shrinks with T and even with an applied bias $|U| < \Delta/e$ some quasiparticles can tunnel due to thermal energy (Kuznetsov, 2001).

When a superconductor (SC) and a semiconductor (SeC) are in electrical contact and form an SeCSC interface, a variety of different phenomena and transport processes can happen. In a device containing multiple SeCSC interfaces, both local (Andreev reflection) and nonlocal (charge imbalance) processes can occur (Klein, 2010).

6. Conclusion

In the "HTSC - SeC" system can be formed three principal types of HCS's (Bunda et al., 1996): tunneling(1), proximity(2) and combined(3).

The bismuth oxyhalide single crystals are layered 2D structured materials. The crystal structure of BiOX is very similar to the symmetry of space groups P4/mmm and/or I4/mmm, where are usual for the $YBa_2Cu_3O_{7-\delta}$ and $Bi(Tl,Hg)_2Sr(Ba)_2Ca_{n-1}Cu_nO_{2n+4}$ HTSC's. Besides, the BiOX crystals, as well as a HTSC's contain oxygen. The thermal expansion and the lattice constants mish-match in the (001) base plane are in good agreement with the same parameters of the HTSC's. Also, the BiOX crystals are good "sparring partners" for the fabrication of "HTSC – photosensitive semiconductor" hybrid contact structure.

The transition of a high temperature superconductor in the superconducting state leads to a significant increase in the photosensitivity of the semiconductor layer of the heterostructure. This is due to single spin quantum tunneling processes of the Cooper pairs inside the semiconductor layer. Also observed the N - shaped anomalies in the temperature dependences of the conductivity (resistivity) in the vicinity of the superconducting transition.

Thus, we believe that based on "high-temperature superconductor - photosensitive semiconductor" hybrid contact structures can be created entirely new device of cryophotoelectronics.

7. References

Bunda, V.V. (1991). Specification of the temperature behavior of the resistance of heterojunctions from high-temperature superconductors with degenerate semiconductors near T_c. *Pis'ma v Zhurnal Tekhnicheskoi Fiziki (written in Russian)*, Vol. 17, No.22 (December 1990), pp. 15-18, ISSN 0320-0116

Akani, M., Froese, A., Staikov, G., Lorenz, W.J.,Röhner, M., Hopfengärter, R. & Saemann-Ischenko, G. (1995). Low-temperature behaviour of high-T_c superconductor / semiconductor heterojunctions. *Physica C,* Vol.245, No.1-2, (December 1994), pp. 131-138, ISSN 0921-4534

Deng, Zhengtao, Chen,Dong, Peng, Bo & Tang, Fangqiong. (2008). From bulk metal Bi to two-dimensional well-crystallized BiOX (X = Cl, Br) micro- and nanostructures: synthesis and characterization. *Crystal growth & design*, Vol.8, No.8 (May 2008), pp. 2995-3003, ISSN 1528-7483

Bunda, V.V., Bunda, S., Krivsky, V., Butorin, A. & Zihika, V. (1996). Physical properties of "HTSC-photosemiconductor" hybrid contact structures. *Czechoslovak Journal of Physics*, Vol. 46, No. 3 (November 1995), pp. 1361-1362, ISSN 0011-4626

Bunda, V., Bunda, S., Vashchuk, F., Feher, A. & Kovač, J. (2010). Physical properties of "HTSC/ Photosemiconductor" micro- and nanoplates based junctions. *Acta Physica Polonica A*, Vol. 118, No.5 (November 2010), pp. 1040-1041, ISSN 0587-4254

Bunda, V., Bunda, S., Kajnakova, M., Feher, A., Syrkin, E. & Feodosyev, S. (2010). Low temperature specific heat of BiOX (X=Cl, Br and I) single crystals. *Acta Physica Polonica A*, Vol. 118, No.5 (November 2010), pp. 986-987, ISSN 0587-4254

Bunda, V., Bunda, S., Kajnakova, M., Feher, A., Syrkin, E. & Feodosyev, S. (2011). Low-temperature specific heat of single crystal bismuth oxyhalides. *Low temperature physics*, Vol.37, No. 4 (July 2010), pp. 326-328, ISSN 1063-777X

Bletskan, D.I., Kopinets, I.F., Rubish, I.D., Turyanitsa, I.I. & Shtilikha, M.V. (1973). Photoconductivity and photoluminescence in BiOCl crystals. *Soviet Physics Journal*, Vol.16, No.5 (May 1973), pp.646-648 ISSN 1064-8887

Bunda, V.V. (1989). Optical anisotropy of deep recombination centers in the layered crystals of the matlokyte family. *Ukrainskii Fizicheskii Zhurnal (Russian Edition),* Vol.34, No.5 (December 1988), pp. 663-666, ISSN 0503-1265

Bunda, V.V. (2005). Functional detectors of radiation for the middle ultraviolet area based on bismuth oxyhalide single crystals. *In: Physics of Electronic Materials. 2nd International Conference Proceedings. Kaluga. Russia. May 24-27,* Vol.2, pp. 3940-3942

Ganesha, R., Arivuoli, D. & Ramasamy, P. (1993). Growth of some group V-VI-VII compounds from the vapour. *Journal of crystal growth*, Vol.128, No.1-4 ,pp.1081-1085 ISSN 0022-0248

Burton, V.K., Cabrera, N. & Frank, F.C. (1951). The growth of crystals and the equilibrium structure of their surfaces. Philosophical transaction of the royal society, Vol.243, No.866 (June 1951), pp.299-358, ISSN 1471-2962

Beck, H.P. & Beyer, T. (1997). Lattice potentials as an instrument in crystal chemistry. II. Applications to the crystal bulk. *Zeitschrift für Kristallographie*, Vol. 221, No.8(December 1996), pp. 565-571, ISSN 0044-2968

Keramidas, K. G., Voutsas, G.P. & Rentzeperis, P. I. (1993). The crystal structure of BiOCl. *Zeitschrift für Kristallographie*, Vol. 205, No. Part-1 (January 1992), pp. 35-40, ISSN 0044-2968

Bercha, D.M., Puga, G.D. & Borets, A.N. (1973). Two-phonon processes in crystals of D_{4h}^{7} symmtry. Physica Status Solidi (B), Vol.55, No.1 (January 1973), pp.69-78 ISSN 0370-1972

Zhang, Ke-Lei, Liu, Cun-Ming, Huang, Fu-Qiang, Zheng, Chong & Wang, Wen-Deng (2006). Study of the electronic structure and photocatalytic activity of the BiOCl photocatalist. Applied Catalysis B: Environmental, Vol.68, No.3-4 (August 2006), pp.125–129, ISSN 0926-3373

Shivagan, D.D., Shirage, P.M. & Pawar, S.H. (2004). Studies on the fabrication of $Ag/Hg_1Ba_2Ca_1Cu_2O_{6+\delta}/CdSe$ heterostructures using the pulse electrodeposition technique. *Semiconductor Science and Technology*, Vol.19, No.3 (September 2003), pp. 323-332, ISSN 0268-1242

Shivagan, D.D., Shirage, P.M. & Pawar, S.H. (2002). Studies on photoinduced effects in pulse-electrodeposited Ag/Hg-1212/CdSe hetero-nanostructures. *Pramana–Journal of physics*, Vol.58, No.5&6 (May 2002) pp. 1183-1190, ISSN 0304-4289

Alfeev, V.N. & Neustroev, L.N. (1990). The photo-current in the tunnel contact: high-temperature superconductor-semiconductor-semiconductor. *Doclady Akademii Nauk SSSR (Reports of the Soviet Academy of Sciences -in Russian)*, Vol.311, No. 5 (Yanuary 1990), pp. 1106-1110, ISSN 0002-3264

Alfeev, V.N., Men'shov, V.N. & Neustroev L.N. (1991). Photoelectric amplification in the tunneling structure degenerate semiconductor/high-temperature superconductor/insulator/metal. *Fizika Nizkich Temperatur (Low Temperature Physics - in Russian)*, vol.17, No.1 (November 1990), pp. 128-130, ISSN 0132-6414

Kleine, A. (2010). *Experiments on nonlocal processes in NS devices.* Inauguraldissertation zur Erlangung der Würde eines Doktors der Philosophie vorgelegt der Philosophisch-Naturwissenschaftlichen Fakultät der Universität Basel, UNI, Basel, Schwizerland, 108 p.

Kuznetsov, G.V. (2004). Transport of the charge carrier through superconductor – semiconductor contact. *Fizika Nizkich Temperatur (Low Temperature Physics - in Russian)*, vol.30, No.10 (April 2004), pp. 1038-1044, ISSN 0132-6414

Kuznetsov, G.V. (2002) Charge carrier passing through the metal-superconducting semiconductor contact. *Fizika i technika poluprovodnikov (Semiconductors – in Russian)*, Vol.39, No.9 (February 2002), ISSN 0015-3222

Kuznetsov, G.V. (2001) Thermoelectrical current through the metals – superconducting semiconductor contact. Pisma v ZETF (JETP Letters - in Russian), Vol.74, No.10 (October 2001), pp. 556-559, ISSN 0021-3640

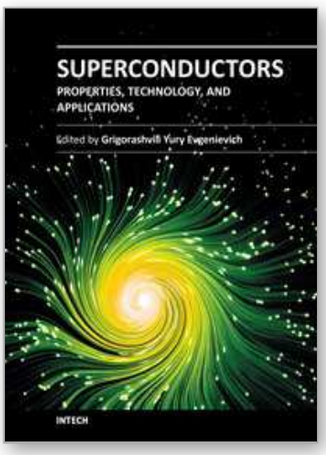

Superconductors - Properties, Technology, and Applications
Edited by Dr. Yury Grigorashvili

ISBN 978-953-51-0545-9
Hard cover, 436 pages
Publisher InTech
Published online 20, April, 2012
Published in print edition April, 2012

Book "Superconductors - Properties, Technology, and Applications" gives an overview of major problems encountered in this field of study. Most of the material presented in this book is the result of authors' own research that has been carried out over a long period of time. A number of chapters thoroughly describe the fundamental electrical and structural properties of the superconductors as well as the methods researching those properties. The sourcebook comprehensively covers the advanced techniques and concepts of superconductivity. It's intended for a wide range of readers.

How to reference
In order to correctly reference this scholarly work, feel free to copy and paste the following:

Viktor V. Bunda and Svitlana O. Bunda (2012). Applications of Superconductor/Photosemiconductor Contact Structures in Electronics, Superconductors - Properties, Technology, and Applications, Dr. Yury Grigorashvili (Ed.), ISBN: 978-953-51-0545-9, InTech, Available from: http://www.intechopen.com/books/superconductors-properties-technology-and-applications/applications-of-superconductor-photosemiconductor-contact-structures-in-electronics

INTECH
open science | open minds

InTech Europe
University Campus STeP Ri
Slavka Krautzeka 83/A
51000 Rijeka, Croatia
Phone: +385 (51) 770 447
Fax: +385 (51) 686 166
www.intechopen.com

InTech China
Unit 405, Office Block, Hotel Equatorial Shanghai
No.65, Yan An Road (West), Shanghai, 200040, China
中国上海市延安西路65号上海国际贵都大饭店办公楼405单元
Phone: +86-21-62489820
Fax: +86-21-62489821

IntechOpen